Local web buckling mechanism and practical design of double-coped beam connections

Michael C. H. Yam[a], Cheng Fang[b]*, Angus C. C. Lam[c]

[a] *Department of Building & Real Estate, The Hong Kong Polytechnic University, Hung Hom, Kowloon, Hong Kong SAR, China*

[b] *Department of Structural Engineering, School of Civil Engineering, Tongji University, Shanghai 200092, China.*

[c] *Department of Civil & Environmental Engineering, University of Macau, Macau SAR, China*

*Corresponding author: email: chengfang@tongji.edu.cn, Tel: +86 21 65983894

Abstract: This paper presents a comprehensive investigation on local web buckling mechanism and design of double-coped beam connections. Following a careful validation study, a series of finite element (FE) models are established, covering a spectrum of geometric and material variables including cope length, cope depth, web slenderness, and steel grade. The study reveals that the main failure mode of the models is either inelastic or elastic local web buckling, and the considered parameters can evidently influence the buckling capacity. The models with short copes tend to fail by inelastic buckling accompanied by excessive shear yielding. For the models with long copes, especially for those with thin webs and high steel grades, stable post-buckling equilibrium path could be sustained after the occurrence of initial buckling, and as a result the ultimate reaction can be evidently higher than that governed by elastic buckling. In addition, stress concentration is significant near the cope corners, and the peak elastic stress concentration factor (SCF) could achieve around 2.0. A further discussion is made on various support and boundary conditions, and these variables are also shown to have clear influences on the local web buckling capacity of double-coped beams. Based on the numerical results, and recognising the potential limitations of the existing design rule, a modified design method, taking account of the various influential factors revealed in this study, is finally proposed. The available experimental and numerical results show that the modified method can effectively improve the accuracy of local web buckling design for double-coped beam connections.

Keywords: Double-coped beam; connections; local web buckling; numerical study; design methods.

1. Introduction

In typical steel structures such as building frames and steel bridges, the same elevation of beam/girder flanges at member intersections is often required to facilitate the fabrication of flooring,

decking, and ceiling systems. In this case, part of the flange of secondary beams often needs to be coped/notched at the beam ends in order to avoid interference of the connected structural members at these junctions. Depending on the structural and architectural requirements, one flange (normally the top one) or both flanges of the beam and the affected part of the web need to be removed, as shown in Fig. 1(a), and hence the strength and stiffness of the beam (with either tee or rectangular shaped reduced section at the coped region) are inevitably reduced. In the absence of the support and restraint from the flange, accompanied by complex stress distributions in the coped web due to geometric discontinuity, a number of local failure modes which are not common in the case of uncoped beams may occur in coped beam connections.

Local web buckling, a failure mechanism mainly arising from the instability of the laterally unrestrained coped edge under compressive action, is one of the most common local failure modes for coped beam connections [1]. Other possible local and global failure modes include block shear [2-6] and lateral torsional buckling [7-10]. The local buckling behaviour of coped web was investigated by a number of researchers. Cheng et al. [11] and Cheng and Yura [12] first conducted a series of full-scale tests on top flange single-coped beam connections, where it was confirmed that local web buckling was the main failure mode for these specimens. Numerical studies were subsequently carried out, based on which a set of design rules was developed for elastic local web buckling design of single-coped beam connections. The design method, which was later adopted by the AISC Steel Construction Manual [13], used a basic plate buckling calculation model to reflect the local web buckling phenomenon. An alternative approach, based on a shear buckling calculation model, was proposed by Yam et al. [14] through conducting more tests and numerical studies on single-coped beam connections. The new model was proposed based on the finding that the buckling line (i.e. the line through which local out-of-plane deflection is propagated due to local buckling as shown in Fig. 2) of the specimens was similar to that typically induced by plate shear buckling and the corresponding predictions were found to agree better with the test results. Aalberg and Larsen [15] also initiated a series of investigations on local web buckling response of coped beams. Six tests were carried out first where the coped beam end was seated on a cylindrical bearing such that a simply-supported condition

2

was produced. Through studying the test results and by conducting additional FE analysis, a new design model was developed by Aalberg [16]. More test data were recently reported by Aalberg [17], where the focus was on aluminium coped beams. The test results confirmed that the design model proposed by Yam et al. [14] could provide good predictions of the local web buckling capacity of single-coped beam connections. Recognising the negative effects caused by the presence of copes, reinforcing strategies were also proposed by some researchers [18-19]. Various stiffener types were considered and examined through experimental and numerical studies, and beneficial effects of these reinforcing strategies were illustrated.

While the previous research has provided insight into the local web buckling behaviour of top (compressive) flange single-coped beams, the relevant information on double-coped beam connections are quite limited. The design of double-coped beam connections may need to be carefully treated as more significant reduction of local web buckling capacity can be induced due to the removal of both beam flanges. Cheng et al. [11] first conducted some numerical studies on such connections and put forth a set of preliminary design rules. It was suggested that the ultimate local web buckling capacity could be safely predicted by checking the flexural yielding, shear yielding, and elastic local buckling capacities of the reduced section. Test evidence was not available until lately, where Aalberg [17] conducted two tests on aluminium double-coped beams. It was found that the design method proposed by Cheng et al. [11] could lead to inconsistent test-to-predicted ratios, and in particular, the connection type (e.g. end-plate or angle cleat connections) was shown to have influence on the local web buckling capacity; however, this was not reflected in the existing design rules [11-13]. More recently, a research programme was launched by the authors and co-workers aiming to fill the knowledge gap in understanding the local web buckling behaviour, design, and reinforcing strategies of double-coped beam connections. The first research stage [20], involving 11 full-scale tests which covered a spectrum of coping details, was recently completed and it was shown that the cope length, cope depth, and coped end connection stiffness could be important variations affecting the buckling resistance. However, the test-to-predicted ratios showed a high level of inconsistency where overly conservative predictions were observed for some specimens whereas unsafe results could be obtained

for some others. This highlighted the need for more rational design rules developed for double-coped beam connections.

This study is an important continuation of the previous experimental programme [20] towards more in-depth understanding of the local web bucking response of such connections and finally the stipulation of a comprehensive set of design guidance. In this paper, after achieving satisfactory agreement between the available test results and the corresponding numerical predictions, an extensive parametric study is carried out examining 144 basic models covering a spectrum of geometric and material variables, including cope length, cope depth, web slenderness, and steel grade. The influences of initial imperfection, coped end connection rotational stiffness, connection type, and lateral bracing conditions over the beam, are also discussed in detail. Based on the results from the numerical study, a modified design approach, building on the conventional design framework proposed by Cheng et al. [11], is proposed and verified via comparisons against the existing test data pool.

2. Modelling strategy and validation

2.1 Test data selected for model validation

The test data from two independent research programmes, one conducted by the authors and co-workers [20], and the other one carried out by Aalberg [17], were employed to validate the FE modelling strategy. For completeness of the current paper, both test programmes are briefly introduced herein. The investigation conducted by the authors and co-workers [20] consisted of 11 full-scale tests on double-coped S460 steel beam connections with the cope length-to-beam depth (c/D) ratio varying from 0.201 to 1.382 and the cope depth-to-beam depth (d_c/D) ratio ranging from 0.063 to 0.126 (key symbols are given in Fig. 1(b)). End-plate connections were adopted for all the specimens. The cope length and depth were reflected in the test code; for instance, C80dc25 indicated that the specimen had the coping dimension of $c = 80$ mm and $d_c = 25$ mm. Local web buckling was observed as the main governing failure mode for most specimens, but two specimens, C80dc25 and C80dc35, failed due to the formation of plastic hinge at the loading point. Aalberg [17] also carried out a series

of tests on coped beams made of aluminium. Two specimens, among a total of 18, were double-coped beam connections, and two connection types, namely, end-plate connection (specimen A10) and double-cleat angle connection (specimen A11), were used. For the former case, the end-plate was directly seated on a load cell, such that a fully rotationally flexible condition was allowed at the coped end; for the latter case, the two angles were bolted to a supporting frame, a more realistic condition in building frames. More detailed geometric dimensions and boundary conditions of these specimens can be found in the literature [17, 20]. The key properties of the specimens are also reproduced in Table 1, where measured values are given unless stated otherwise.

2.2 Modelling strategy

The general finite element (FE) programme ABAQUS [21] was used to simulate the test specimens. Both material and geometric nonlinearities were considered in the FE analysis. The S4R elements, i.e. 4-node shell elements with reduced integration, were used to discretise the structural members, and the general meshing size was approximately 10 mm × 10 mm with a refined mesh of 5 mm × 5 mm for the coped web region and the connections. The nonlinear material property of steel and aluminium was simulated by using the isotropic hardening model with the von Mises yield criterion. Idealised trilinear stress-strain responses, reflecting the yield and ultimate strengths and the corresponding strains, were adopted for the material model. The key material properties were obtained from the coupon test results, and were then converted to true stress/strain in ABAQUS. For the case of end-plate connections, the weld between the end-plate and coped web end was simulated via a 'tie' interaction with no weld failure being considered [22]. When double cleat angle connections were considered, the contacting surface between the angle leg and the coped web was also idealised by a 'tie' interaction. It should be noted that although the angle legs and the web were actually connected via bolt lines, the local load transferring mechanism (by bolt) should have limited influence on the overall local web buckling behaviour (provided that no shear failure occurs); therefore, the 'tie interaction' could still be a reasonable assumption reflecting the local restraining effect provided by contacted angle leg. Other boundary conditions (lateral bracing) were appropriately defined to reflect

the actual conditions of the test setup. The typical model and its meshing scheme and boundary conditions are illustrated in Fig. 2(a).

The FE analysis consisted of two major steps, which were 1) buckling analysis (eigenvalue analysis), and 2) nonlinear load-deflection analysis [23]. In the first step, the buckling modes of the models could be obtained, where the fundamental mode, as typically shown in Fig. 2(a), is usually the one being of great interest from an imperfection assessment point of view. The second step was performed to trace the nonlinear responses of the models under the applied load, and the first/fundamental buckling mode obtained from the first step was selected as the predefined initial imperfection shape, noting that the amplitude of the imperfection can be scaled to any desired value to cater for imperfection sensitivity analysis. Since the imperfection conditions were not fully measured in the test programmes, four levels of initial imperfection amplitude, namely, $0.01t_w$, $0.1t_w$, $0.3t_w$, and $0.5t_w$ (where t_w is the thickness of the web) were considered in the validation study.

2.3 Model validation

The predicted reaction-deflection responses of the specimens examined by the authors and co-workers [20] are compared with the test results as shown in Fig. 3(a). The two specimens that failed by full beam section yielding are not included in the figure. Good agreements are generally observed between the FE predictions and the test results. The initial imperfection amplitude is shown to have moderate influences on the ultimate reaction of the models with relatively short copes (e.g. $c = 80$ mm or 150 mm), and these specimens generally failed by inelastic buckling. However, for those with longer copes and tended to fail by elastic local web buckling, little imperfection sensitivity is exhibited, which is due to the development of post-buckling resistance. The presence of post-buckling mechanism in these specimens has been confirmed in the preliminary numerical study reported in [20], and further discussions will be made in Section 3. The typical failure modes (especially the buckling pattern) of the models are shown in Fig. 2(b), where good agreements are observed between the FE predictions and the test observations.

The predicted reaction-deflection responses of the two aluminium specimens studied by Aalberg [17] are shown in Fig. 3(b). As the test reaction-deflection curves were not directly given in

the literature, only the reported ultimate reaction is shown in the figure. It is observed that the ultimate reactions for both specimens are reasonably predicted by the FE models, and again, a certain level of imperfection sensitivity is exhibited. It seems that the FE prediction tends to slightly overestimate the ultimate reaction for specimen A10. This is probably due to the fact that in the FE model, a pin support was considered along the bottom edge of the end-plate, i.e. the end-plate was free to rotate, but lateral movement of the end-plate was not allowed. For the test case, however, the end-plate was cut with a V-shaped bottom edge which was simply rested above the load cell, in which case minor lateral movement might be induced when local web buckling occurred. This effect was not accurately reflected in the FE model as it is very difficult to fully simulate the contact condition (e.g. friction coefficient) between the V-shaped edge and its support. Nevertheless, the local buckling mechanism is well captured by the FE models, and the buckling pattern for both specimens also agrees very well with the test observation reported in Aalberg [17].

3. Parametric study

3.1 Parameter matrix

Having shown that good agreements exist between the FE predictions and the available test results, a parametric study was carried out to further examine the local web buckling behaviour of double-coped beams with varying coping details and boundary conditions. The current study commences with the analysis of 144 basic models, covering a spectrum of parameters including cope length (c), cope depth (d_c), material property/grade, and web thickness (t_w). Towards more comprehensive design recommendations, further discussions are made on the influences of connection type and lateral bracing conditions through performing additional analyses, as detailed later in Section 4. A reference steel beam, UB406×140×39, was employed for the numerical study, and in the interest of consistency, the loading and supporting conditions were the same as those adopted in the test programme conducted in [20], as discussed in the previous validation study. The considered cope length ranged from 80 mm to 500 mm and cope depth varied from 25 mm to 75 mm, leading to the cope length-to-beam depth (c/D) and cope depth-to-beam depth (d_c/D) ratios ranging from 0.201 to

1.256 and from 0.063 to 0.188, respectively. These coping geometries could well cover the general conditions encountered in practice. Four web thicknesses (t_w), which are 4 mm, 6.4 mm (nominal value for UB406×140×39), 8 mm, and 10 mm, were considered for the reference beam, enabling a wider range of coped web slenderness to be considered. As a further expansion of the parameter matrix, three steel grades were considered for each geometric configuration, namely, S355, S460, and S690. The steel grades represent the cases of both normal steel and high-strength steel (HSS), noting that HSS beams (especially fabricated I-section beams) have been receiving great attention recently [24], but very limited study has been conducted on local failures of these members due to the presence of cope. The key symbols and geometric configurations of the models for the parametric study are shown in Fig. 1(b).

For the in-plane boundary conditions, existing studies [17, 20] suggested that the rotational stiffness provided by the coped end connection could affect the local web buckling capacity. In the current study, a consistent end-plate connection detailing, as illustrated in Fig. 1(b), was employed, such that the results can be interpreted in a consistent manner. The geometric configuration of the end-plate (8 mm thick, with S355 steel) might represent a class of typical beam-to-column and beam-to-beam connection types in building frames, and based on the FE prediction, the end-plate connection can offer a rotational stiffness of approximately 503 kNm/rad under a pure bending condition. For the far end (uncoped end) of the beam model, an idealised roller-supporting condition was assumed. Furthermore, it was assumed that the top flange of the beam was braced laterally, which may reflect the case of composite flooring system. The influence of other lateral bracing conditions will be discussed in Section 4.

For ease of discussion, each model was designated with a model code. The code starts with the cope length and depth, followed by the web thickness, and ends with the steel grade. For example, C80dc25T6.4S355 represents the model with coped length c = 80 mm, cope depth d_c = 25 mm, web thickness t_w = 6.4 mm, and steel grade = S355. The modelling strategy of these models was similar to those discussed in the previous validation study. In particular, for the modelling of steel, the key material properties, i.e. Young's modulus E, yield strength f_y, and ultimate strength f_u, were based on

the nominal values recommended in Eurocode 3 [25-26]. In addition, the strain at ultimate strength ε_u for S355 and S460 steel was assumed to be 15% [25], while that for S690 steel was assumed to be 10% [27]. Moreover, based on the finding that an initial imperfection amplitude of $0.1t_w$ could lead to reasonable agreements between the FE predictions and test results, this level of imperfection was adopted for the parametric study.

3.2 General response

The FE results show that the coped end ultimate reactions (R_u) of the models can vary significantly, ranging from 25.2 kN to 1380.4 kN with different coping details. For most models, the main failure mode is local web buckling (either inelastic or elastic), as indicated by the development of a buckling line originating from either the top cope corner or the top edge of the coped web. At ultimate load, the maximum lateral movement/displacement of the coped web (i.e. normally the location where the buckling line starts), δ_u, tends to increase with increasing cope length. For the case of short copes (e.g. c = 80 mm or 150 mm), δ_u is not considerable and is usually less than 2 mm. However, after reaching the ultimate load the displacement starts to increase quickly. For the models with longer copes (especially for those with thin webs) a much larger value of δ_u can be sustained at ultimate load (normally more than 15 mm). It is noted that for some models with very 'stocky' coped web, i.e. those with relatively small cope length (e.g. c = 80 mm) and thick web (e.g. t_w = 10 mm), evident plastic shear deformation of the coped web panel can be induced. For this type of failure, the applied load keeps increasing after the initial shear yielding of the coped web (due to the strain hardening effect) with no sign of local web buckling until the development of very excessive shear deformation. After reaching the ultimate load, a buckling line originating from the top cope corner is exhibited over the web panel, a phenomenon which is similar to that observed in the other models with less stocky coped web.

3.3 Load-deflection response

The typical load vs. in-plane deflection (P-Δ) responses of representative models are shown in Fig. 4, where the occurrence of local web buckling is also marked in the curves via yellow filled

circles. The geometries of the selected models cover the considered range of cope length (from 80 mm to 500 mm) as well as the three material grades, such that the key influential factors can be well reflected. The fundamental-mode buckling load (P_{cr}) of the models (obtained from the eigenvalue analysis) is also included in the figures to enable further interpretation of the FE results. It is generally shown that the load-deflection curves of the models follow a linear ascending load path in the initial loading stage, but the subsequent non-linear responses vary significantly with changing coping details and material properties. For ease of interpretation in the following discussions, the 'occurrence of local web buckling' indicates the stage when the maximum lateral deflection of the top cope edge (i.e. the location where the buckling line is initiated) starts to be developed quickly; 'stable' post-buckling resistance indicates that the load can keep increasing after the occurrence of local web buckling, such that the ultimate load, which is achieved at the post-buckling stage, exceeds the initial local web buckling load; 'unstable' post-buckling resistance indicates that the load starts to decrease after the occurrence of local web buckling.

For the case of $t_w = 4$ mm (as shown in Fig. 4(a)), the sustained load drops 'abruptly' after reaching the ultimate load for the models with the shortest cope length (i.e. C80dc50T4 series), and subsequently unstable post-buckling equilibrium path is exhibited. When the cope length is increased to 150 mm (i.e. C150dc50T4 series), a similar trend of the P-Δ curves is observed with varying steel grades, although the influence of steel grade on the ultimate load seems to be less significant. Again, unstable post-buckling equilibrium path is exhibited. Compared with the C80dc50T4 models, the ultimate loads of the C150dc50T4 models are much closer to the elastic buckling load P_{cr}. This indicates that the buckling mechanism may start to turn from inelastic buckling to elastic buckling when the cope length increases from 80 mm to 150 mm (strain conditions will be discussed in the next section), but due to the presence of imperfection, the critical peak load is still less than the elastic buckling load P_{cr}. When the cope length further increases to 300 mm (i.e. C300dc50T4 series), stable post-buckling equilibrium path starts to be developed, which is signified by the increase of the sustained load after the inception of buckling. The initial buckling occurs at a load level slightly lower than P_{cr}, which is, again, due to the effect of initial imperfection. The different steel grades show little

influence on the initial buckling load, implying an elastic local web buckling mechanism; however, the post-buckling resistance is predominantly affected by the steel grade, where a higher steel grade leads to more considerable post-buckling resistance. For model C300dc50T4S355, the post-buckling resistance is suppressed due to the relatively low steel yield strength, but when the steel grade increases to S460 and S690, the ultimate load (at the post-buckling stage) starts to exceed P_{cr}. When c = 500 mm, more evident post-buckling resistance is exhibited, where the ultimate load can achieve more than twice of P_{cr} (model C500dc50T4S690).

For the models with a thicker web (i.e. t_w = 10 mm), different load-deflection responses are observed, as shown in Fig. 4(b). For the case of shortest cope (i.e. C80dc50T10 series), the initial load-deflection curve is linear; however, due to the occurrence of shear yielding over the coped web, nonlinear load-deflection behaviour is initiated after which the load keeps increasing due to the strain hardening effect. No immediate local web buckling is induced at this strain hardening stage. Subsequently, inelastic local web buckling finally occurs because of excessive plastic shear deformation and the sustained load starts to drop. When the cope length is increased, no such shear yielding is developed, and the failure mode is governed by inelastic local web buckling with flexural yielding. Again, the sustained load starts to drop after initial local web buckling, but it is of interest to find that a minor regaining of the resisting load is exhibited for the models with $c \geq 300$ mm at the post-buckling stage. However, the regained load is quite limited, and therefore the initial buckling load is not exceeded.

3.4 Strain patterns

The buckling mechanism of the models can be further described through the strain conditions developed within the coped web panel. It is noted that all the stresses/strains discussed hereafter are based on the values at the mid-thickness integration point of the shell elements, unless stated otherwise. Fig. 5 gives the equivalent plastic strain (PEEQ) patterns of typical models at the stage when the ultimate load is just reached. In order to clearly show the corresponding deformation state, the maximum lateral deflection of the cope at ultimate load (δ_u) and the location where δ_u occurs, are

11

also marked in Fig. 5. In addition, the major buckling line which is later developed beyond ultimate load is marked by dash lines in the figure. It can be seen that for the models with c = 80mm, shear yielding over the entire coped web section is induced at the ultimate load. Significant strain concentration is developed near the cope corners, and the maximum lateral deflection of the cope δ_u, which is less than 3 mm, occurs near the top cope corner, noting that this is the location where the buckling line is later developed when the unloading starts.

With increasing cope length, the shear stress becomes less critical and flexural yielding/buckling starts to govern the failure mode. For the case of c = 150 mm, the value of δ_u is also limited, and significant stress concentration is observed near the cope corners; again, the subsequent buckling line is initiated from the top cope corner. For the case of c = 300 mm, however, a different buckling mechanism is exhibited. The maximum lateral deflection of the cope is observed at approximately 1/4 to 1/3 length of the top cope edge from the end of cope. The location of δ_u generally coincides with the location where the buckling line is subsequently induced, and at ultimate load, δ_u is already considerable (more than 6 mm). However, yielding has not been developed at ultimate load near the location of δ_u, which indicates that the models failed by elastic local web buckling. It is noted that the buckling line is developed immediately after the ultimate load. For the case of c = 500mm, a similar buckling mechanism is observed, although δ_u is more significant at ultimate load. It is of interest to note that for model C500dc75T6.4S460, post-buckling resistance is developed, and the ultimate load, which exceeds the initial buckling load, is achieved at the post-buckling stage. Importantly, it is found that δ_u at ultimate load can achieve 50.7 mm, which suggested that a stable post-buckling equilibrium path can be accompanied by excessive lateral deformation of the top cope edge.

In order to show the stress concentration effect in more detail, Fig. 6 gives the typical elastic bending stress (longitudinal stress) distribution along the top cope edge. The calculated stress (My/I), which excludes the stress concentration effect, is also included in the figure. The stresses are illustrated in a normalised manner. It is confirmed that significant stress concentration is developed

near the cope corner, and the peak stress concentration factor (SCF) is observed along the top cope edge at around 10 mm from the end of cope, which corresponds to the location near the edge of the radius of the rounded cope corner. The models with varying coping geometries generally show a similar level of peak SCF (around 2.0). The increases of the cope length and cope depth seem to slightly decrease the value of SCF, but the influence is marginal. Towards the end of the cope, the SCF decreases again, and the value at the end of the cope is generally less than 1.3.

3.5 Influence of parameters

Four main parameters, namely, cope length, cope depth, web thickness, and steel grade, were considered for the basic models, and their influences on the ultimate coped end reaction (R_u) are shown in Fig. 7 (in a normalised manner). Owing to a large parameter matrix being considered, only typical trends are reflected in the figure. It can be seen that the increase of cope length, which as a result increases the 'buckling length' of the compressive cope edge, can significantly decrease R_u (as shown in Fig. 7(a)). For instance, when the cope length is increased from 80 mm (c/D = 0.201) to 300mm (c/D = 0.754), R_u can be decreased by more than 60%. However, it is of interest to find that when the cope length further increases to 500 mm (c/D = 1.256), the decrease of R_u becomes less significant, especially for the model groups with thin webs. In other words, the decreasing rate seems to 'slow down' with increasing cope length, and it is a common trend exhibited by all the considered model groups. As previously discussed, this phenomenon can be attributed to the development of post-buckling resistance for the case of long copes. The cope depth also has evident influence on the local web buckling capacity of the models. As can be seen in Fig. 7(b), R_u can be decreased by approximately 40% when the cope depth is tripled, i.e. d_c being increased from 25 mm (d_c/D = 0.063) to 75 mm (d_c/D = 0.188). The decrease of R_u can be correlated to the decreased section modulus of the reduced coped section, noting that the elastic modulus of the coped web ($t_w h_o^2/6$, symbols having been defined in Fig. 1(b)) is decreased by 49% when d_c is increased from 25 mm to 75 mm. The decrease of section modulus leads to an increased level of compressive stress demand along the top cope edge and thus an increased potential for local web buckling.

Fig. 7(c) shows that the ultimate reaction of the models can be effectively increased by increasing the web thickness t_w. When t_w is doubled, i.e. t_w being increased from 4 mm to 8 mm, R_u can be increased to at least 2.5 fold. In addition, a slightly lower increasing rate is found for the model groups with $c = 80mm$. As discussed previously, those models, especially those with relatively thicker webs, experience significant shear yielding prior to local web buckling, and therefore the benefit of increasing t_w for local web buckling capacity can be less obvious. Increasing the steel grade can also benefit the local web buckling capacity, but it may be less effective than increasing the web thickness. As shown in Fig. 7(d), when the steel grade is increased from S355 to S460 (f_y being increased by 30%), R_u is on average increased by around 15%. When the steel grade is further increased to S690 (f_y being increased by 94% compared with S355), R_u is increased by up to 80%. It is also observed that the increasing rate (with increasing steel grades) can vary evidently for different comparison groups, and the variation is due to the different and complex failure modes (e.g. shear yielding, elastic buckling, inelastic buckling, and post-buckling responses) for different groups of model. Taking the C150dc50T4 and C150dc50T10 series for instance (square and inverted triangle blue solid dots shown in Fig. 7(d)), limited increase of R_u with increasing steel grade is found for the former group because these models with a thin web tend to fail by elastic buckling (with no post-buckling resistance, as previously discussed in Section 3.3), and therefore the influence of steel grade is not remarkable. When the web thickness is increased to 10 mm, however, inelastic buckling starts to govern the failure mode, a case which shows greater dependence on the material property. It is also worth mentioning that for the case of $c = 500$ mm, although the models tend to fail by elastic buckling, the influence of steel grade is still obvious. This is due to the development of post-buckling resistance which is, again, dependent on steel grade.

4. Further discussions

4.1 Influence of connection rotational stiffness

In practical design, depending on specific requirements and designers' preference, the connections used for coped beam end may vary. This inevitably leads to different levels of rotational

stiffness offered by various connections, which would have an influence on the local web buckling capacity of coped beams. The possible influence of connection rotational stiffness lies in the fact that a negative bending moment can be induced at the coped region with increasing connection stiffness, and this effect tends to decrease the 'effective buckling length' along the top cope edge and as a result mitigates the potential for local web buckling [20]. The possible influence of connection stiffness on local web buckling capacity is examined in this section. In order to vary the stiffness without changing any other parameters, the Young's modulus of the end-plate was deliberately adjusted in order to achieve the desired stiffness levels. The connection stiffness can be quantitatively measured via FE simulations. As mentioned, a consistent rotational stiffness was employed for the end-plate connection considered in the basic models. The calculated rotational stiffness of the end-plate connection from the FE results was 503 kNm/rad (mentioned in Section 3.1). Four levels of stiffness were additionally considered, namely, idealised pin (free to rotate), 2000 kNm/rad, 5000 kNm/rad, and fully rigid. Representative model groups were selected, and the influence of connection stiffness on the ultimate reaction R_u is shown in Fig. 8(a). Again, the trend of R_u is shown in a normalised manner.

It is confirmed that the increase of connection stiffness can increase the local web buckling capacity of double-coped beams, and the increasing rates of R_u varied with different cope lengths. Limited beneficial effect is observed for the models with $c = 80$ mm, and this is due to the fact that the R_u of these models are mainly governed by shear yielding of the coped web, and this failure mechanism is generally not affected by the connection rotational stiffness. With increasing cope length, inelastic local web buckling starts to dominate, and thus the presence of the negative moment can benefit the buckling resistance. When elastic local web buckling gradually governs the failure mode for the models with long copes, more evident increase of R_u is observed with increasing connection stiffness due to the significant decrease of the 'effective buckling length' along the top cope edge. The most evident increase of R_u is observed for the case of $c = 500$ mm, where the R_u of the model with a rigid connection can reach more than twice of that with an idealised pin connection.

An interesting yet important finding is that, when the fully rigid connection is employed, the calculated range of negative moment is approximately 218 mm from the coped beam end, which

15

exceeds 150 mm. Therefore, it is intuitively deduced that local web buckling is not likely to occur for the models with relatively short copes (i.e. c = 80 mm and c = 150 mm) as their top cope edge, based on the 'theoretical' bending moment diagram, is subjected to tension. However, local web buckling is still a major failure mode that governs R_u for these models. In order to explain this phenomenon, Fig. 9(a) shows the load-deflection response of model C150dc50T6.4S460 (with fully rigid connection) and the corresponding bending stress patterns at different loading stages. For easy interpretation, only tension and compression stresses are distinguished in the stress contour, i.e. black for tension stress and light grey for compression stress. It can be seen that at the elastic stage, tension and compression stresses are developed at the upper and lower parts of the coped web, respectively, which is coherent with the fact that negative moment is induced by the rigid connection. Minor lateral deflection is first induced over the bottom cope edge, but this 'instability tendency' has no influence on the load carrying capacity, and the sustained load keeps increasing which is accompanied by a gradual change of the stress pattern, where compression stress is gradually developed near the top cope corner from which buckling line is then originated and propagated. More complex stress patterns are shown at late loading stages beyond ultimate load. Due to a larger load level being resisted with the increase of the connection stiffness, the occurrence of local web buckling may also be accompanied by shear buckling. This can be indicated by the formation of a compression strut at the peak load, and once local buckling occurs, a tension strut with an approximately 45° incline angle is shown.

4.2 Influence of connection type

End-plate (i.e. the reference case considered in the basic models) and angle cleat connections are two connection types that are commonly used for building frames. The use of angle cleat can provide partial lateral restraints for the coped web, a case which may benefit the local web buckling capacity. In order to investigate this effect, two types of angle cleat connections, namely, double-angle cleats and single-angle cleat, were examined. The length of the 'side angle leg' i.e. the part that is attached to the coped web, was taken as 75 mm. The main reason to consider the single-angle cleat connection type was to examine the possible influence of out-of-plane loading eccentricity e. The value of e is taken as 80 mm in this study, as illustrated in Fig. 8(b). For consistency, the same in-

plane rotational stiffness was considered for the different connections types, which was achieved by adjusting the Young's modulus of the angle leg that is attached to the column face. The modelling approach for the angle cleats was the same as that discussed in the validation study.

According to the normalised ultimate reactions (R_u) shown in Fig. 8(b), the lateral restraining effect offered by the angle leg can indeed benefit the local web buckling capacity. R_u can be increased by at least 7% when the double-angle connection is used instead of the end-plate connection. A significant increase of R_u is observed for the case of $c = 80$ mm, and this is due to the fact that the length of the angle leg (75 mm) effectively covers the most part of the coped web, and thus significant retraining effect is provided against local web buckling. With increasing cope lengths, the lateral restraining effect contributed by the 75 mm-long angle leg becomes less predominant. When the single-angle connection is employed, R_u can be decreased. The lateral restraining effect provided by the angle leg may still benefit the local web buckling capacity, but this can be counteracted by the detrimental effect of the out-of-plane eccentricity. As a result of the combined effects, R_u can be decreased to a value which is lower than that of the model with end-plate connections. Nevertheless, the decrease of R_u is not considerable (by 10% at most). The typical local buckling response of the models with the angle cleat connections are shown in Fig. 9(b).

4.3 Influence of lateral bracing

For the basic models, the top flange of the steel beam is laterally braced, an assumption which can be realistic for the case of composite beams or other beam elements where lateral movement of the top flange is not allowed. However, some members (e.g. bare steel beams) may not be fully braced laterally along the entire beam length, and as a result the local web buckling performance of these beams may be different. In order to study this effect, the lateral bracings of selected models were removed, except for the load application point which normally represents a member junction where lateral restraint exists. The normalised ultimate reactions of the typical models with the two different bracing conditions are given in Fig. 8(c). It can be clearly seen that the exclusion of the lateral bracing can decrease the local web buckling capacity by more than 10%. The typical deformed shapes (top view) of the laterally unbraced models are shown in Fig. 9(c), where it is found that lateral movement

is induced at the top flange, and as result, local web buckling is less effectively 'restrained' by the top flange. Moreover, it is observed that (not shown in the figures) the post-buckling resistance (i.e. regaining of sustained load beyond initial buckling), which is developed in model C500dc50T6.4S460 with lateral bracing, is not exhibited for its laterally unbraced counterpart. This implies that the lateral restraining effect offered by the top flange could facilitate the development of post-buckling resistance.

Generally speaking, the above-mentioned boundary conditions, including connection rotational stiffness, connection type, and lateral bracings, can affect the local web bucking capacity of double-coped beams, and these effects may need to be incorporated into relevant design rules, as will be discussed in Section 5.

5. Design considerations

5.1 Existing design method

The current design rule stipulated in the AISC Steel Construction Manual [13] stems from the early numerical study conducted by Cheng et al. [11], where it was recommended that the ultimate reaction R_u of double-coped beam connections could be obtained by taking the minimum capacity of three load resistance mechanisms, namely, flexural yielding, shear yielding, and elastic local web buckling of the coped web. The flexural yielding capacity R_y is determined based on the assumption that failure occurs upon 'first yielding' of the coped web (excluding stress concentration), and therefore the ultimate reaction R_y can be simply obtained by $R_y = M_y/c$, where M_y = elastic yield moment of the coped web, and c = cope length. The shear yielding capacity R_{vy} is obtained by $R_{vy} = f_y A_w / \sqrt{3}$, where f_y = yield strength of web, and A_w = cross-sectional area of the coped web. For elastic local web buckling capacity R_{cheng}, the critical moment M_{cr} was determined by assuming a lateral-torsional plate buckling model with an unbraced length of c and a linearly-increased bending moment diagram, as expressed by:

$$M_{cr} = f_d \left(\frac{\pi}{c} \right) \sqrt{EI_y GJ} \tag{1}$$

Where E = Young's modulus, $I_y = h_o t_w^3/12$, G = shear modulus, $J = h_o t_w^3/3$, and f_d = an adjustment factor to ideally consider some influential factors including the effects of stress concentration and shear-bending interaction, and the value is taken as $f_d = 3.5 - 7.5(d_c/D)$ (relevant dimensions and symbols for the above equations have been defined in Fig. 1(a)). Similar to the design method for flexural yielding, the ultimate reaction R_{cheng} can be obtained by $R_{cheng} = M_{cr}/c$. The lowest value of R_y, R_{vy}, and R_{cheng} governs the design.

Employing the existing design method, the resulting FE-to-predicted ratios are obtained, varying from 0.618 to 4.091 for the 144 basic models. The mean value of the FE-to-predicted ratios is 1.413, and the coefficient of variation (CoV) is 38.2%. These data indicate that the design predictions are inconsistent, and they are overly conservative for some models, but can be quite unsafe for some other cases. Fig. 10(a) shows the direct comparisons between the FE results and existing design predictions along with the 10% and 15% discrepancy lines, where a high level of discrepancy is clearly observed. According to the previous discussions, the discrepancy could be caused by the following limitations of the existing design method: 1) the calculation of R_y and R_{vy} took no account of stress concentration, stress redistribution, and strain hardening effects; 2) elastic buckling analysis was performed for the derivation of R_{cheng}, but no detailed nonlinear analysis was conducted. In particular, no post-buckling resistance was considered for the case of 'slender' coped webs; 3) possible interactions among the three failure mechanisms (i.e. related to R_y, R_{vy}, and R_{cheng}) could render separate design resistance inaccurate; and 4) the influence of various boundary conditions were not considered in the existing design method. Therefore, more rational design approaches, which can potentially address the above limitations, are desirable.

5.2 Development of modified design method

Considering that the design method proposed by Cheng et al. [11] has been continuously serving the design community in the past two decades and its procedure is quite straightforward, therefore, it is decided to retain the existing design framework, i.e. R_{design} = minimum of (R_y, R_{vy}, R_{cheng}), but to make appropriate modifications on each checking item to address the aforementioned

issues and limitations. The modification schemes for the three failure mechanism are recommended as follows.

- Design for flexural yielding resistance R_y

According to the existing design method, flexural yielding governs the ultimate capacity of 75 models (out of 144). The FE analysis shows that these models generally fail by inelastic local web buckling. It is also found that R_y becomes conservative when the web thickness t_w is increased. This is due to the fact that 'stocky' coped webs are less susceptible to local buckling, and significant yielding is normally developed before ultimate load. As a result, the value of R_y, which is calculated based on the first yielding of the coped web section, underestimates the actual flexural yielding resistance. On the other hand, less conservative predictions are observed when the steel grade is increased, and for some models with HSS (e.g. S690), R_y can be unsafe. Moreover, more conservative predictions are observed when the cope depth is increased. Based on these findings, an adjustment factor, ψ_y, is proposed for R_y, as expressed in the following form to reflect the above-mentioned trends:

$$\psi_y = \left(C_1 + C_2 \frac{t_w}{h_o} \right) \left(\frac{355}{f_y} \right)^{C_3} \tag{2}$$

where C_1, C_2, and C_3 are constants which are set aiming to provide good agreements with the FE results. A trial-and-error procedure, making the average FE-to-predicted ratio close to unity (slightly on the conservative side) and the associate CoV minimised, was adopted to determine the appropriate values of the three constants, and it is preliminarily recommended that $C_1 = 0.65$, $C_2 = 25$, and $C_3 = 0.3$. The modified design flexural yielding resistance, $\psi_y R_y$, leads to much more consistent design predictions, as discussed later in Section 5.3.

- Design for shear yielding resistance R_{vy}

Shear yielding only governs the failure mode of the models with very short copes. According to the existing design method, 24 models (C80 series) fail by shear yielding, and it is shown that R_{vy} can provide reasonable predictions. However, an issue is that for the models with relatively smaller t_w, R_{vy} tends to be unsafe, especially for those with HSS. This may be attributed to the fact that the

combined effect of shear and bending and the stress concentration effect causes earlier yielding of the web at the cope corner and hence reduce the inelastic buckling capacity of the models. On the other hand, R_{vy} can be conservative for the models with larger t_w due to the exclusion of the beneficial shear strain hardening effect in the shear yielding resistance design. The cope depth has little influence on the shear yielding mechanism of the coped section. Based on these observed tendencies, shear yielding resistance R_{vy} may be modified by an adjustment factor ψ_{vy} as given by:

$$\psi_{vy} = \left(C_1 + C_2 \frac{t_w}{D} \right) \left(\frac{355}{f_y} \right)^{C_3} \tag{3}$$

where D = uncoped beam depth. Similar to the design strategy for flexural yielding, $C_1 = 0.7$, $C_2 = 17$, and $C_3 = 0.3$ are recommended for Eq. (3) which leads to good agreement with the FE results.

- Design for local web buckling resistance R_{cheng}

According to the predictions from the existing design method, R_{cheng} governs the local web buckling resistance of the models with relatively slender coped webs. It is observed that R_{cheng} is generally safe for these models, but neglecting the post-buckling resistance could make R_{cheng} overly conservative for those with small web thickness and high steel grade (e.g. $t_w = 4$ mm with S690 steel). In addition, more conservative predictions are observed when the cope length is increased. Considering these trends, an adjustment factor ψ_{cheng} is proposed, as expressed by:

$$\psi_{cheng} = \left(C_1 + C_2 \frac{c}{h_0} \right) \left(\frac{f_y}{355} \right)^{C_3} \left(\frac{0.01D}{t_w} \right)^{C_4} \tag{4}$$

and again through a trial-and-error procedure, $C_1 = 0.4$, $C_2 = 1.1$, $C_3 = 0.5$, and $C_4 = 1.15$ are recommended which provide good agreements with the FE results.

- Additional design considerations for boundary conditions

Three adjusting coefficients, β_s, β_t, and β_b, are additionally proposed to take account of the effects of varying boundary conditions including connection rotational stiffness, connection type, and lateral bracing condition, respectively. In light of the discussions in Section 4, the increase of the rotational stiffness of the beam end connection could benefit the local web buckling capacity, where

more evident influence is observed for the models with longer copes. Based on the trend shown in Fig. 8(a), the following preliminary equation for β_s is proposed via curve fitting:

$$\beta_s = \left(0.89 + 1.08\frac{c}{D}\right) - \left(-0.14 + 1.27\frac{c}{D}\right)0.8^R \tag{5}$$

where R = connection rotational stiffness (unit: 10^3 kNm/rad), and the value can be obtained via FE analysis. In practical design, designers may also want to use analytical models, such as the component method stipulated in Eurocode 3 [28], to calculate the initial stiffness of commonly used connections. Moreover, connection types are found to influence the local web buckling capacity of the models, and based on the available FE results, β_t is preliminarily taken as:

$$\beta_t = 1.15 \text{ for double angle connection} \tag{6}$$

$$\beta_t = 0.9 \text{ for single angle connection} \tag{7}$$

Finally, the removal of the lateral bracings along the beam could compromise the local web buckling capacity, and it is suggested that β_b may be taken as:

$$\beta_b = 0.8 \tag{8}$$

It should be noted that the values recommended in this section are provisional ones which are based on the limited FE data reported in this paper, and they are determined aiming to match the FE findings and tend to be on the conservative side. The rationale behind these coefficients may need to be further validated through more extensive experimental and numerical investigations, and designers are encouraged to use the proposed coefficients only for the cases that fall within the current range of parameters. Moreover, these coefficients may be used following a simple 'linear law', and any complex interactions among the effects of connection rotational stiffness, connection type, and lateral bracing condition are not considered.

5.3 Proposed design procedure

Building on the existing design framework proposed by Cheng et al. [11], and employing the above design approaches for the three basic failure mechanisms, the local web buckling capacity of double-coped beam connections can be obtained by taking the minimum value of $\psi_y R_y$, $\psi_{vy} R_{vy}$, and

$\psi_{cheng}R_{cheng}$. Therefore, the design local web buckling resistance (unfactored) can be calculated in the following final form:

$$R_{design} = \beta_s\beta_t\beta_b R_{min} \tag{9}$$

where R_{min} = the minimum of $\psi_y R_y$, $\psi_{vy}R_{vy}$ and $\psi_{cheng}R_{cheng}$. Using the modified design method, the comparisons between the FE results and design predictions are shown in Fig. 10(b). While the maximum observed discrepancy is 23% (on the conservative side), the discrepancies for most models are within 15%. The mean FE-to-predicted ratio obtained by the modified design method is 1.070, which is close to unity, and the corresponding CoV is only 6.8%. Recalling that the conventional design method leads to a mean FE-to-predicted ratio of 1.413 and the CoV of 38.2%, it can be seen that the modified method provides much more reasonable predictions. To further verify the modified design method, the local web buckling capacity of the test specimens conducted by the authors and co-workers [20] and Aalberg [17] are predicted using the above-mentioned design procedure, as detailed in Table 2. It is clearly seen that the modified design method leads to better agreements between the predicted and test results. The mean test-to-predicted ratio using the conventional design method ($R_u/R_{d,con}$) is 1.30 for the considered specimens and the corresponding CoV is 29.4%; when the modified design method is employed, the mean test-to-predicted ratio ($R_u/R_{d,mod}$) is 1.05, which is much closer to unity, and the CoV decreases to 12.2%. These results show that the modified design method can effectively improve the accuracy of prediction of the local capacity of double-coped beam connections. Finally, it is worth mentioning the final form of the design equation, i.e. Eq. (9), is obtained from curve fitting and is unfactored. For practical design, a resistance factor/partial factor should be added through a reliability analysis based on the mean FE-to-predicted ratio and the corresponding CoV given in this study. This is, however, not within the scope of the current paper but worth future investigations. In addition, it is reemphasized that the design equation is only applicable to members with the current range of parameters.

6. Summary and conclusions

This paper reported an extensive parametric study on local web buckling mechanism and design of double-coped beam connections. A series of finite element (FE) models, which have been validated through comparisons against the available test results, were established, covering a spectrum of geometric and material variables including cope length, cope depth, web slenderness, and steel grade. The main findings and conclusions are noted as follows.

- The main failure mode of the models is local web buckling (either inelastic or elastic), and for some models with short copes (e.g. $c = 80$ mm), inelastic buckling happened accompanied by excessive shear yielding. For the models with long copes (e.g. $c = 500$ mm), especially for those with thin webs and high steel grades, stable post-buckling equilibrium path was observed. In addition, stress concentration was significant near the cope corners, and it was found that the peak elastic stress concentration factor (SCF) could achieve around 2.0.

- In general, the local web buckling capacity of the models increases with increasing web thickness and steel grade, but decreases with increasing cope length and cope depth.

- The increase of connection rotational stiffness is beneficial for local web buckling capacity. It is of interest to find that even when the entire range of cope length was subjected to negative bending moment due to the use of rigid connections, local web buckling could still be a major failure mode governing the ultimate reaction at the nonlinear deformation stage.

- Moreover, the retraining effect offered by double-angle connections could help improve the local web buckling capacity, but this can be counteracted by the detrimental effect of the out-of-plane eccentricity if single-angle connection was used instead.

- The local web buckling capacity of double-coped beams also depends on the lateral bracing conditions along the top flange of the beam. The exclusion of the lateral bracing can decrease the local web buckling capacity by more than 10% compared with the laterally braced beams.

- Recognising the potential limitations of the conventional design method proposed by Cheng et al. [11], a modified design method was proposed for better predictions of local web buckling capacity R_{design} for double-coped beam connections. Building on the existing design framework, appropriate modifications was made on the three checking items, namely, flexural yielding, shear yielding,

and elastic local web buckling capacities, and the additional influences of connection stiffness/type and lateral bracing conditions were considered. The final proposed design equation follows the form of $R_{design} = \beta_s \beta_t \beta_b \min\left(\psi_y R_y, \psi_{vy} R_{vy}, \psi_{cheng} R_{cheng}\right)$.

- The modified design method was shown to have satisfactory agreement with the FE predictions, where the resulting mean FE-to-predicted ratio was 1.070, and the corresponding CoV was 6.8%. Available tests results were also employed to further validate the modified method, where satisfactory agreement was also observed.

7. Acknowledgements

References

[1] Yam MCH, Fang C, Lam ACC, Cheng JJR. Local failures of coped steel beams – a state-of-the-art review. Journal of Constructional Steel Research 2014;102:217-32.

[2] Franchuk CR, Driver RG, Grondin GY. Experimental investigation of block shear failure in coped steel beams. Canadian Journal of Civil Engineering 2003;30(5):871-81.

[3] Driver RG, Grondin GY, Kulak GL. Unified block shear equation for achieving consistent reliability. Journal of Constructional Steel Research 2006;62:210-22.

[4] Topkaya C. Finite element modeling of block shear failure in coped steel beams. Journal of Constructional Steel Research 2007;63(4):544-53.

[5] Fang C, Lam ACC, Yam MCH, Seak KS. Block shear strength of coped beams with single-sided bolted connection. Journal of Constructional Steel Research 2013;86:153-66.

[6] Lam ACC, Fang C, Yam MCH, Wang W, Iu VP. Block shear strength and design of coped beams with double bolt-line connections. Engineering Structures 2015;100: 293-307

[7] Cheng JJR, Yura JA, Johnson CP. Lateral buckling of coped steel beams. Journal of Structural Engineering, ASCE 1988;114(1):1-15.

[8] Lam CC, Yam MCH, Iu VP, Cheng JJR. Design for lateral torsional buckling of coped I-beams. Journal of Constructional Steel Research 2000;54:423-43.

[9] Maljaars J, Stark JWB, Steenbergen HMGM, Abspoel R. Lateral–torsional buckling resistance of coped beams. Journal of Constructional Steel Research 2005; 61(11):1559-75.

[10] Gupta AK. Buckling of coped steel beams. Journal of Structural Engineering, ASCE 1984;110(9):1977-87.

[11] Cheng JJ, Yura JA, Johnson CP. Design and behavior of coped beams. Ferguson Structural Engineering Laboratory Report No. 84-1, Department of Civil Engineering, University of Texas; July 1984.

[12] Cheng JJR, Yura JA. Local web buckling of coped beams. Journal of Structural Engineering, ASCE 1986;112(10):2314-31.

[13] American Institute of Steel Construction. Steel Construction Manual 14th Edition. One East Wacker Drive, Suite 700, Chicago, Illinois, 2011.

[14] Yam MCH, Lam ACC, Iu VP, Cheng JJR. The local web buckling strength of coped steel I-beam. Journal of Structural Engineering, ASCE 2003;129(1): 3-11.

[15] Aalberg A, Larsen PK. Local web buckling of coped beams. In: Proceedings of Nordic Steel Construction Conference NSCC 2001, Helsinki, Finland, 2001.

[16] Aalberg A. Experimental and numerical parametric study on the capacity of coped beam ends. Journal of Constructional Steel Research 2015;113:146-55.

[17] Aalberg A. Design of aluminium beam ends with flange copes. Thin-Walled Structures 2015;94:593-602.

[18] Yam MCH, Lam ACC, Wei F, Chung KF. The local web buckling strength of stiffened coped steel I-beam. International Journal of Steel Structures 2007;7(2):129–38.

[19] Yam MCH, Ma HW, Lam ACC, Chung KF. Experimental study of the strength and behaviour of reinforced coped beams. Journal of Constructional Steel Research 2011;67: 1749–1759.

[20] Fang C, Yam MCH, Lam ACC, Liu YH, Chung KF. Local web buckling of double-coped steel beam connections. Journal of Constructional Steel Research, Submitted.

[21] ABAQUS Analysis User's Manual. ABAQUS Standard, Version 6.12; 2012.

[22] Wang W, Fang C, Qin X, Chen YY, Li L. Performance of practical beam-to-SHS column connections against progressive collapse. Engineering Structures 2016;106:332-47.

[23] Fang C, Yam MCH, Zhou XY, Zhang YY. Post-buckling resistance of gusset plate connections: Behaviour, strength, and design considerations. Engineering Structures 2015;99:9-27.

[24] Mela K, Heinisuo M. Weight and cost optimization of welded high strength steel beams. Engineering Structures 2014; 79: 354–364.

[25] EN 1993-1-1:2005, Eurocode 3: Design of Steel Structures – Part 1-1: General rules and rules for buildings. European Committee for Standardization, Brussels, Belgium, 2005.

[26] EN 1993-1-12:2007, Eurocode 3: Design of Steel Structures – Part 1-12: Additional rules for the extension of EN1993 up to steel grades S700. European Committee for Standardization, Brussels, Belgium, 2007.

[27] Shi G, Ban HY, Bijlaard FSK. Tests and numerical study of ultra-high strength steel columns with end restraints. Journal of Constructional Steel Research 2012;70:236–47.

[28] EN 1993-1-8:2005, Eurocode 3: Design of Steel Structures – Part 1-8: Design of Joints. European Committee for Standardization, Brussels, Belgium, 2005.

List of figures:

Fig. 1 Coped beam connections: a) practical coping details of steel beams, b) key symbols and geometric configurations for parametric study

Fig. 2 Validation study: a) typical FE models and meshing scheme, b) comparisons of buckling mode

Fig. 3 Comparisons of reaction-deflection responses: a) test data reported by Fang et al. [20], b) test data reported by Aalberg [17].

Fig. 4 Typical load-deflection responses: a) $t_w = 4$ mm, b) $t_w = 10$ mm

Fig. 5 Typical equivalent plastic strain (PEEQ) patterns of models at ultimate load

Fig. 6 Typical elastic bending stress distributions along the top cope edge

Fig. 7 Influence of parameters on ultimate reaction: a) influence of cope length, b) influence of cope depth, c) influence of web thickness, d) influence of steel grade

Fig. 8 Further discussions: a) influence of connection rotational stiffness, b) influence of connection type, c) influence of lateral bracing

Fig. 9 Illustrations for further discussions: a) influence of connection rotational stiffness, b) influence of connection type, c) influence of lateral bracing

Fig. 10 Comparisons between FE results and design predictions: a) conventional design method, b) modified design method

List of tables:

Table 1 Specimen details in considered test programmes

Table 2 Comparisons between test results and design predictions

Table 1 Specimen details in available test programmes

	Test specimens	c/D	d_c/D	Cope length c (mm)	Cope depth d_c (mm)	Web thickness t_w (mm)	Web yield strength (MPa)	Web ultimate strength (MPa)	Web Young's modulus (MPa)	Connection type	Failure mode
	C80dc25	0.201	0.063	80	24	6.28	455.9	586.8	192598	EP	PH
	C80dc35	0.201	0.088	80	34	6.33	455.9	586.8	192598	EP	PH
	C80dc50	0.201	0.126	80	49	6.24	485.9	620.6	200866	EP	LWB
	C150dc25	0.377	0.063	150	24	6.30	485.9	620.6	200866	EP	LWB
	C150dc50	0.377	0.126	148	49	6.25	480.7	613.7	190570	EP	LWB
Fang et al. [20]	C450dc25	1.131	0.063	450	24	6.52	459.9	595.6	200356	EP	LWB
	C450dc50	1.131	0.126	450	49	6.39	459.9	595.6	200356	EP	LWB
	C550dc25	1.382	0.063	550	24	6.50	479.9	609.2	197437	EP	LWB
	C550dc35	1.382	0.088	550	34	6.56	479.9	609.2	197437	EP	LWB
	C550dc50	1.382	0.126	550	49	6.28	475.3	607.7	202311	EP	LWB
	C550dc50R	1.382	0.126	550	49	6.40	475.3	607.7	202311	EP	LWB
Aalberg [17]	A10	0.340	0.154	88	40	4.65	258.0^	290.0*	NG	EP	LWB
	A11	0.340	0.154	88	40	4.65	258.0^	290.0*	NG	DAC	LWB

Note:

^ mean value within the web measured from different directions

* read from typical stress-strain curves

EP = end plate, DAC = double-angle cleat, PH = plastic hinge over beam section, LWB = local web buckling, NG = not directly given in the literature

Table 2 Comparisons between test results and design predictions

	Test specimens	Conventional design					Modified design							
		Ultimate Reaction R_u (kN)	R_y (kN)	R_{vy} (kN)	R_{cheng} (kN)	$\dfrac{R_u}{R_{d,con}}$	$\psi_y R_y$ (kN)	$\psi_{vy} R_{vy}$ (kN)	$\psi_{cheng} R_{cheng}$ (kN)	Connection rotational stiffness (10^3 kNm/rad)	β_s	β_t	β_b	$\dfrac{R_u}{R_{d,mod}}$
Fang et al. [20]	C80dc50	353.7	520.3	514.1	1736.5	**0.69**	550.1	449.4	864.5	3.1	1.05	1	0.8	**0.94**
	C150dc25	344.3	389.1	600.4	702.3	**0.88**	385.3	524.9	439.6	4.2	1.16	1	0.8	**0.96**
	C150dc50	272	281.8	507.8	505.4	**0.97**	301.0	447.3	337.0	3.1	1.13	1	0.8	**1.00**
	C450dc25	114.5	130.9	593.0	79.4	**1.44**	132.7	529.4	98.9	0.5	0.95	1	1	**1.22**
	C450dc50	93.4	91.6	484.4	56.8	**1.64**	99.2	432.4	80.0	0.5	0.95	1	1	**1.23**
	C550dc25	84.3	108.2	597.9	54.8	**1.54**	108.3	527.0	81.8	0.5	0.94	1	1	**1.10**
	C550dc35	76.8	96.1	563.7	48.4	**1.59**	98.5	496.8	75.9	0.5	0.94	1	1	**1.08**
	C550dc50	62.1	78.6	507.0	39.6	**1.57**	84.5	449.7	66.5	0.5	0.94	1	1	**1.00**
	C550dc50R	70.2	78.6	507.0	39.6	**1.77**	84.5	449.7	66.5	1.4	1.20	1	1	**0.88**
Aalberg [17]	A10	57.4	69.0	124.1	343.5	**0.83**	77.1	122.7	172.5	0.0	0.99	1	0.8	**0.94**
	A11	93.8	69.0	124.1	343.5	**1.36**	77.1	122.7	172.5	3.9	1.07	1.15	0.8	**1.24**
					Mean=	**1.30**							**Mean=**	**1.05**
					CoV=	**29.4%**							**CoV=**	**12.2%**

Note:

Conventional design prediction $R_{d,con} = \min\left(R_y, R_{vy}, R_{cheng}\right)$

Modified design prediction $R_{d,mod} = \beta_s \beta_t \beta_b \min\left(\psi_y R_y, \psi_{vy} R_{vy}, \psi_{cheng} R_{cheng}\right)$
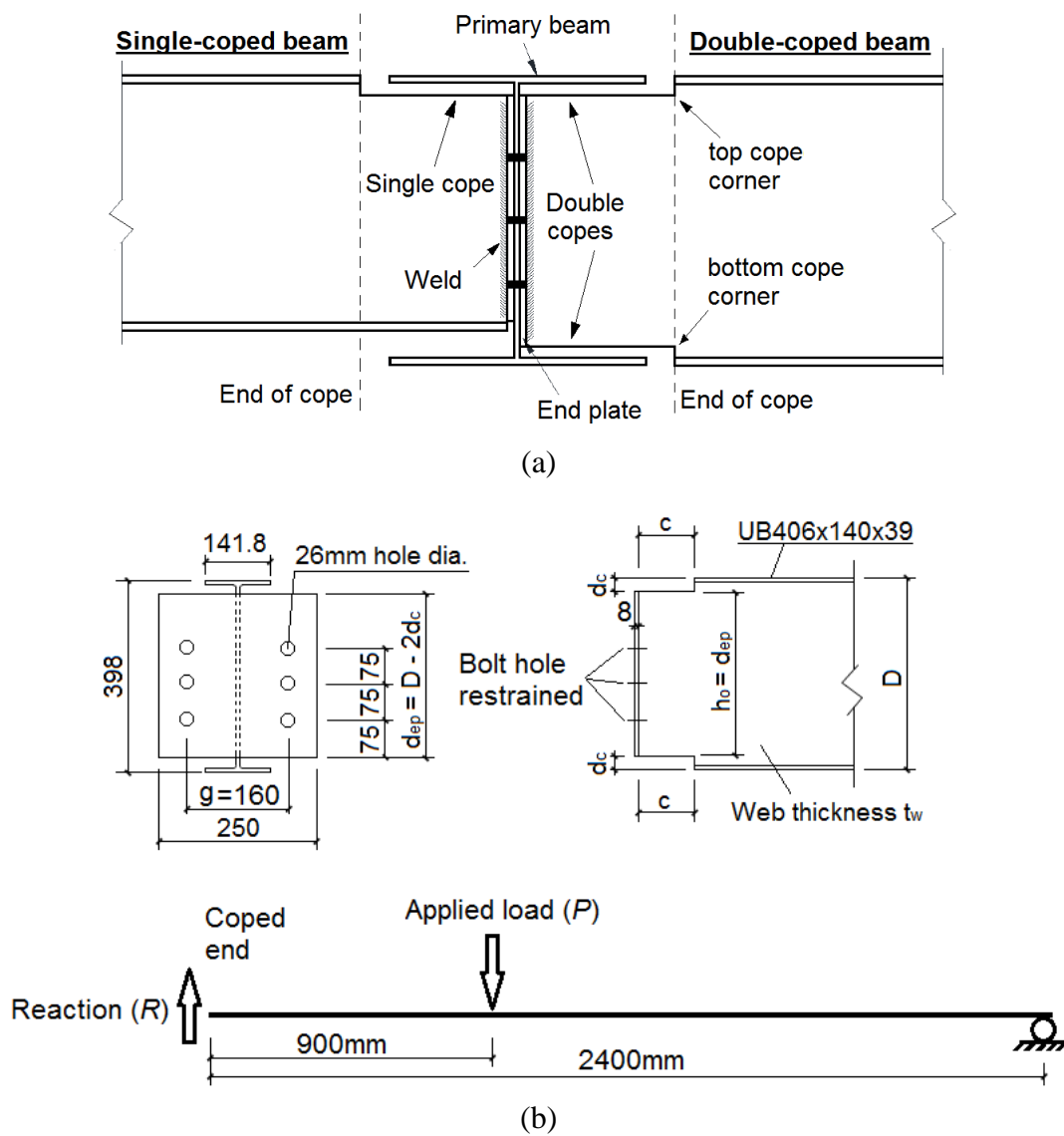
Fig. 1 Coped beam connections: a) practical coping details of steel beams, b) key symbols and geometric configurations for parametric study
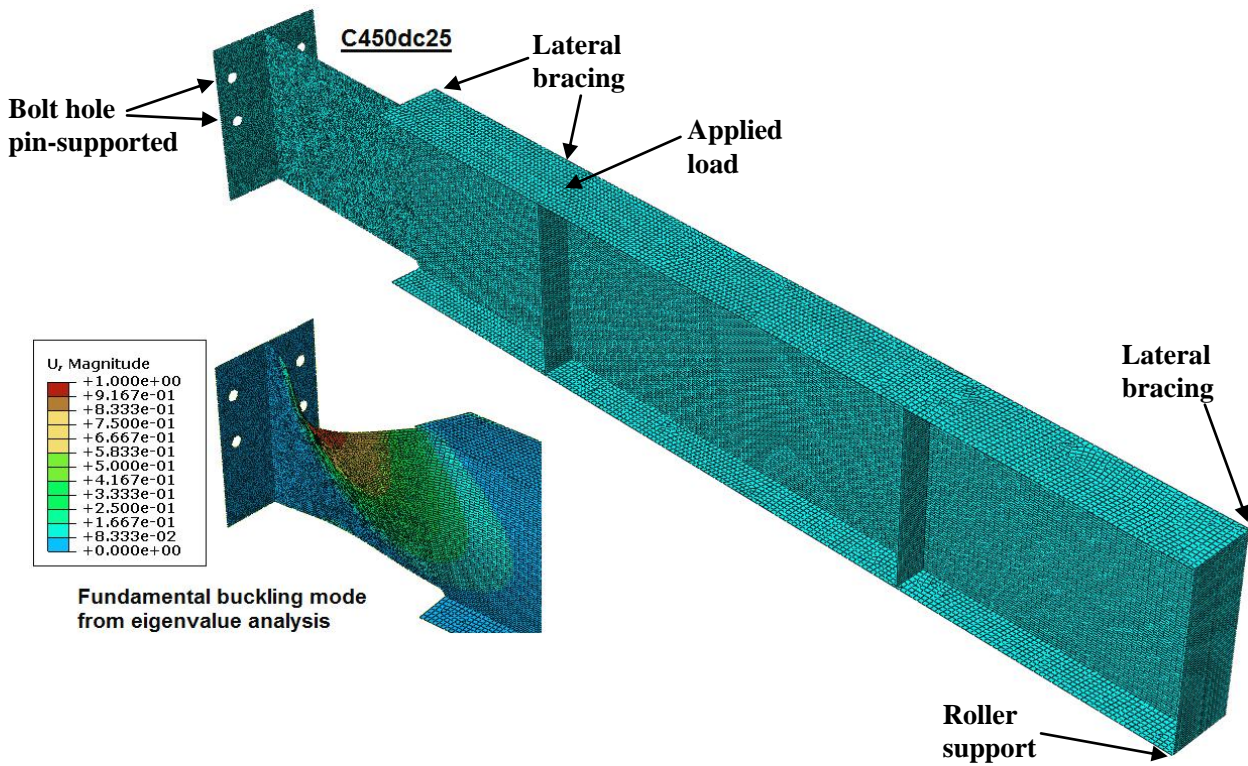
(a)
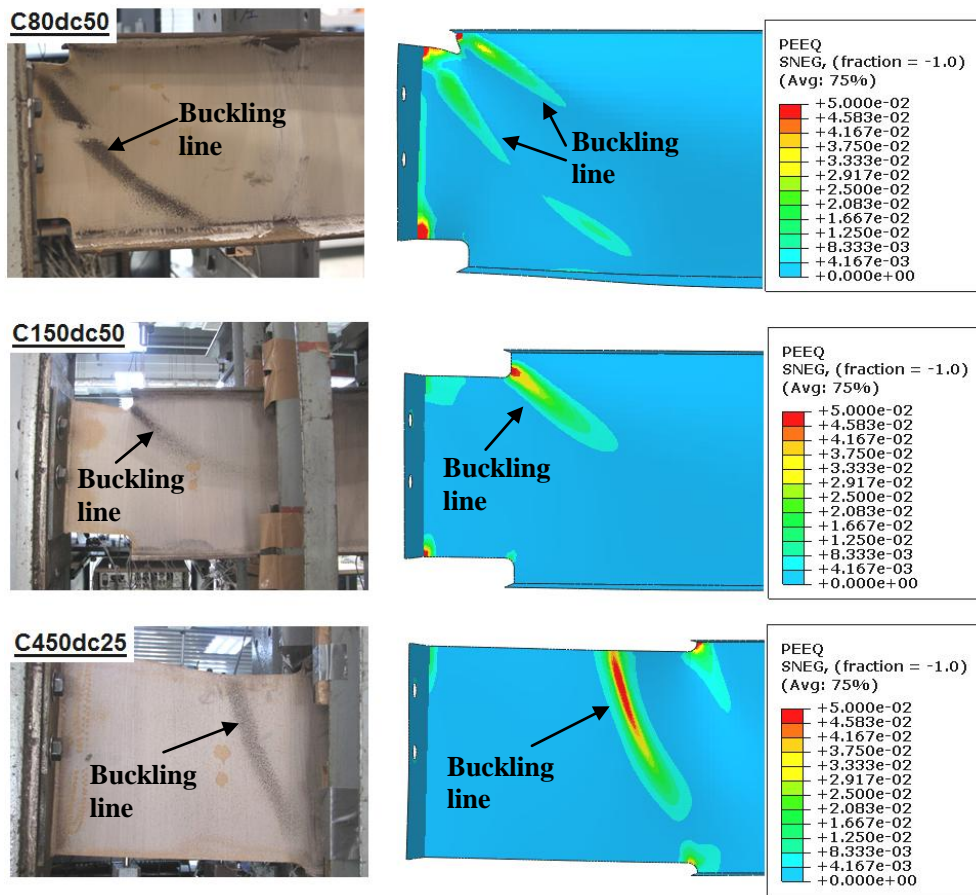
(b)

Fig. 2 Validation study: a) typical FE models and meshing scheme, b) comparisons of buckling mode
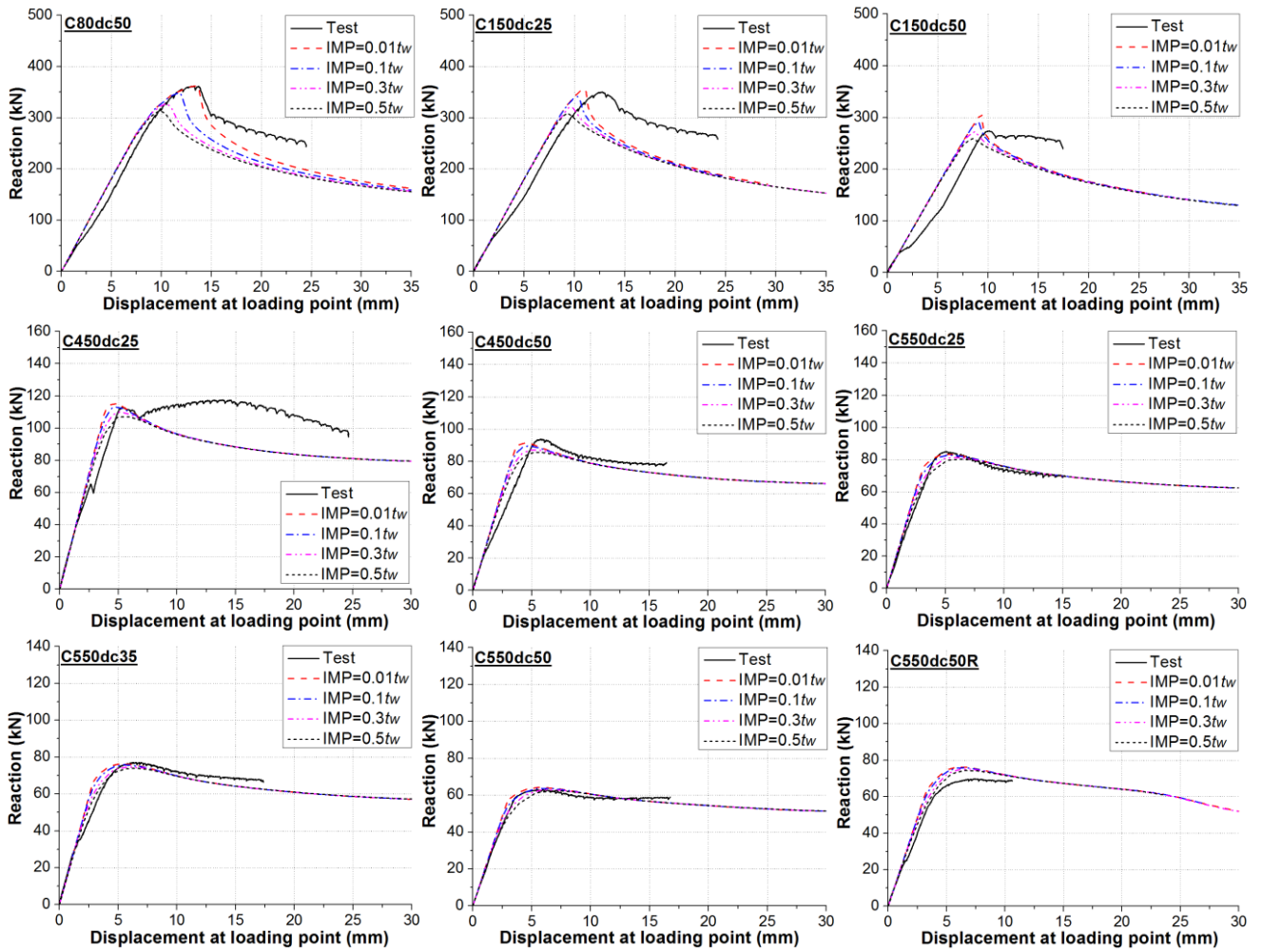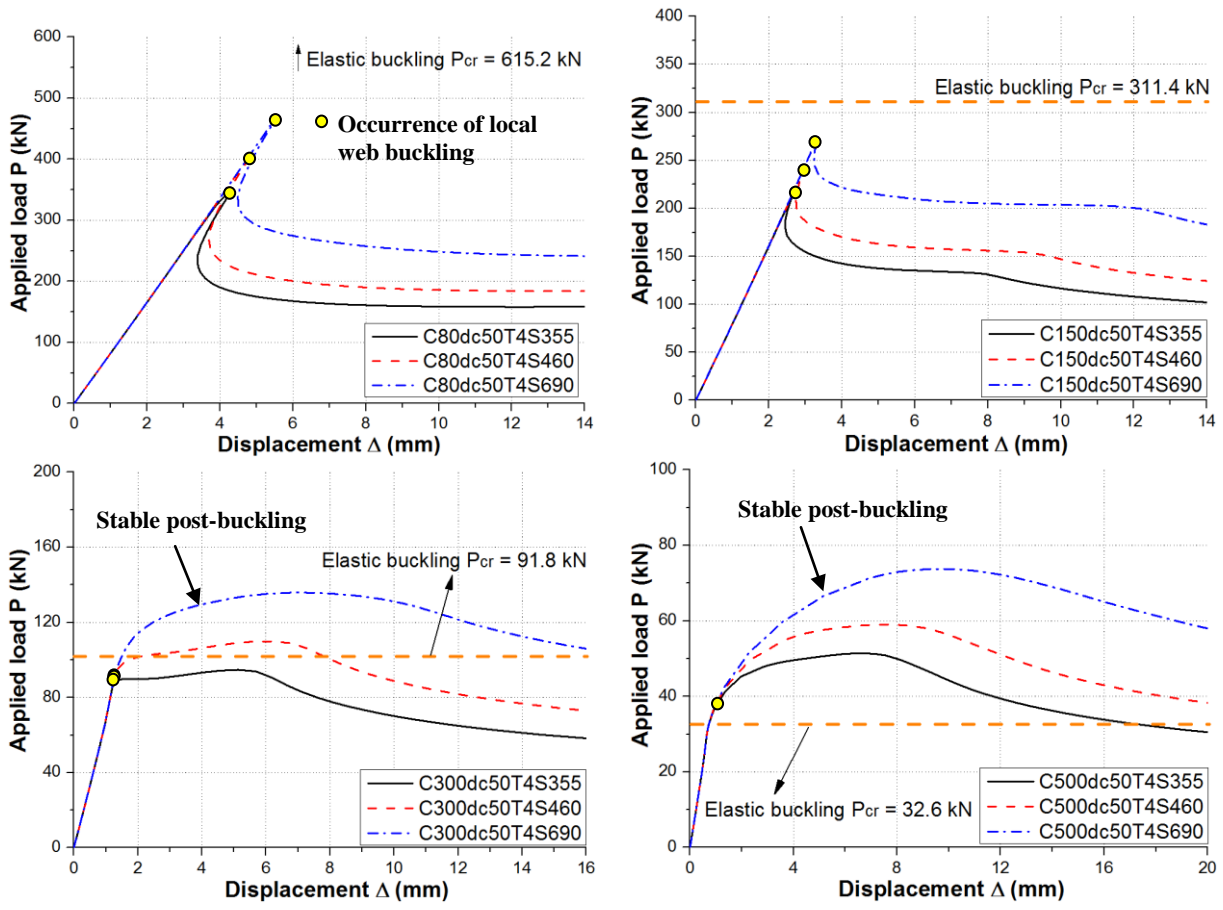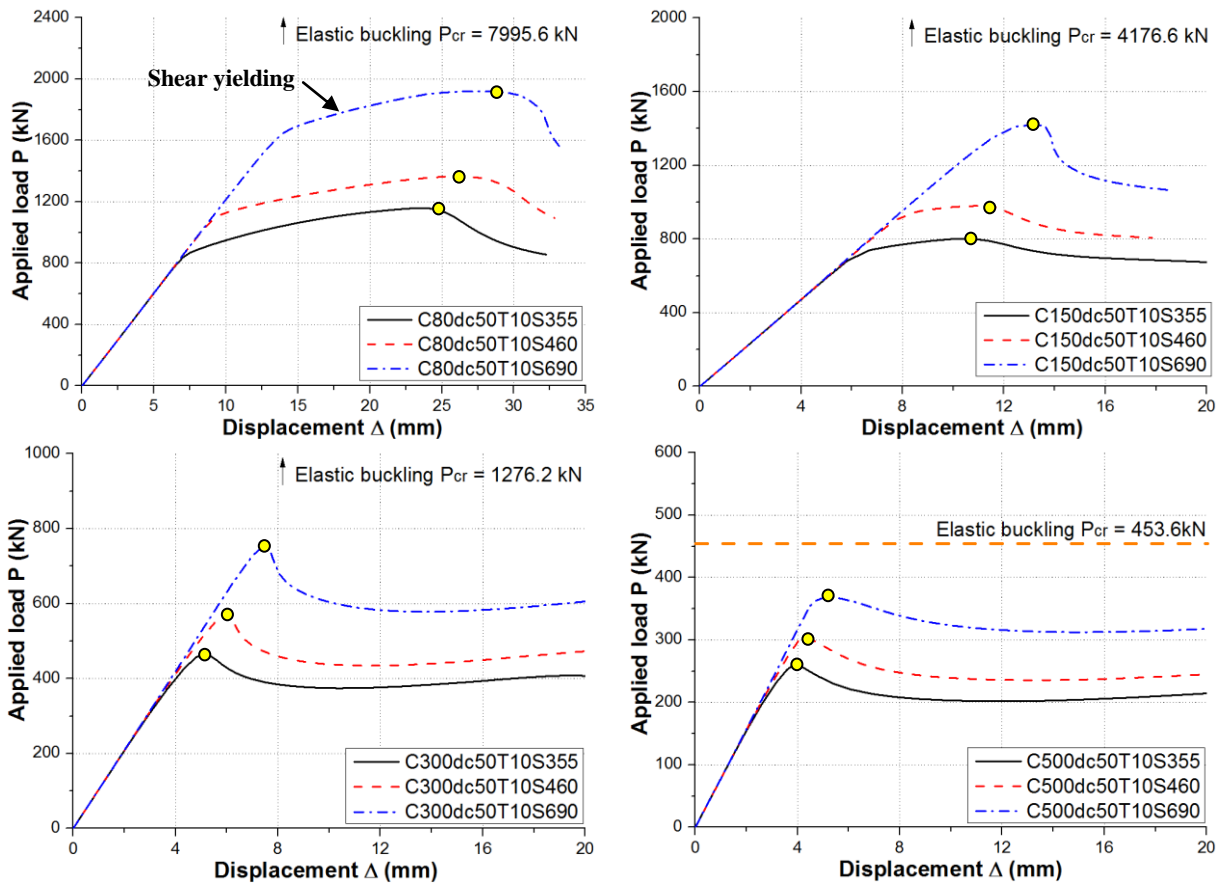
(a)
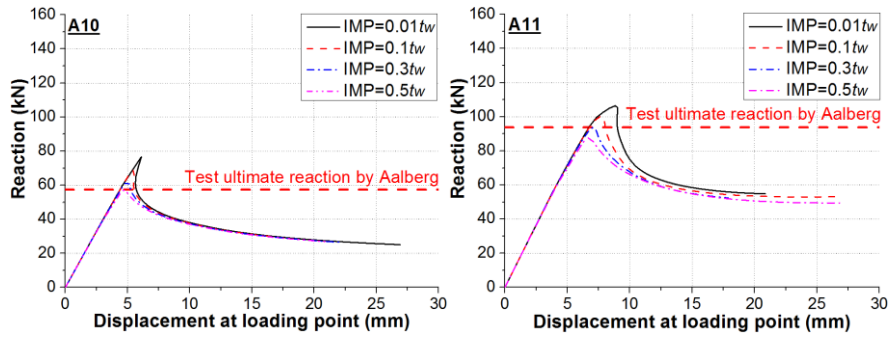
(b)

Fig. 3 Comparisons of reaction-deflection responses: a) test data reported by Fang et al. [20], b) test data reported by Aalberg [17].

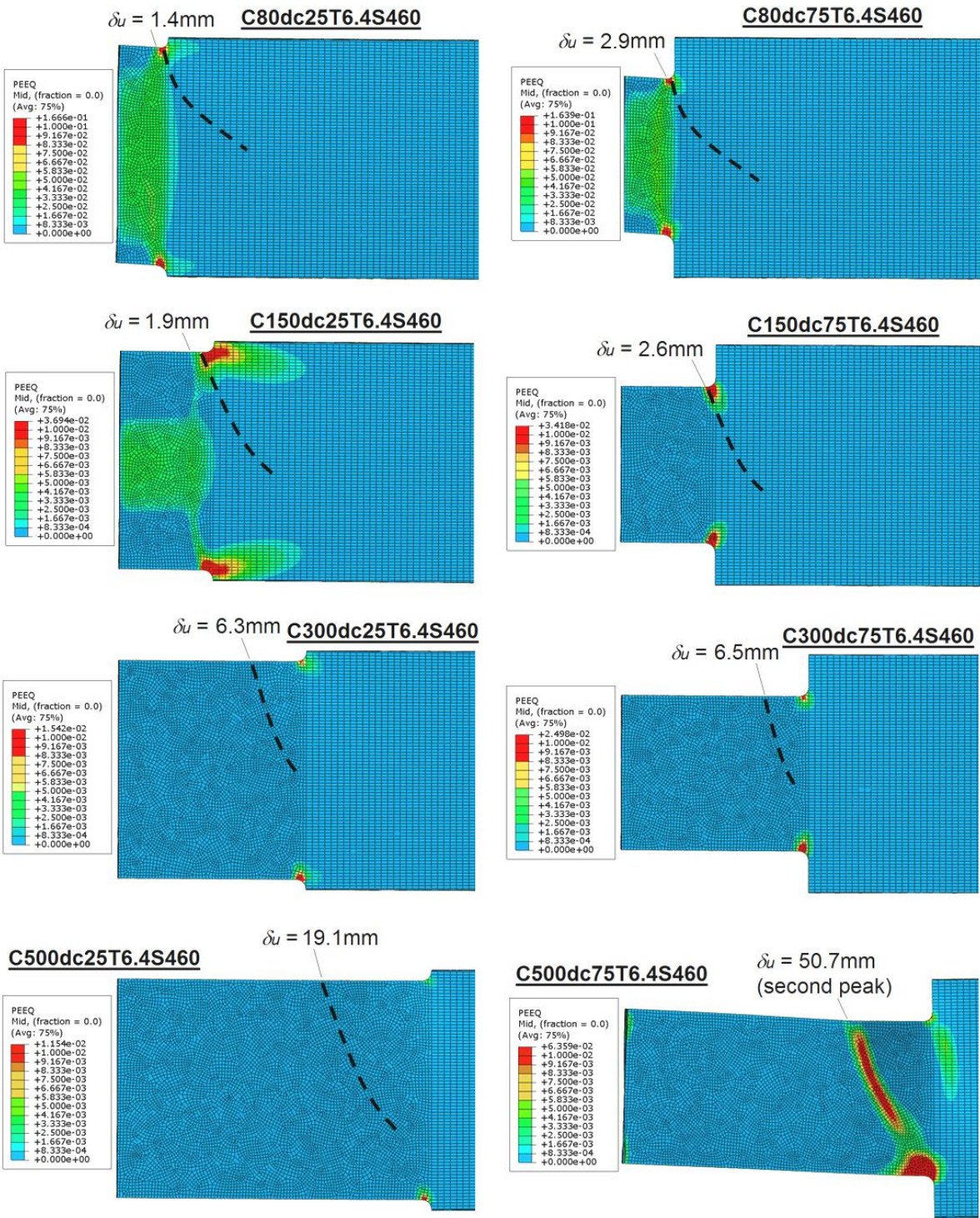**Fig. 4** Typical load-deflection responses: a) $t_w = 4$ mm, b) $t_w = 10$ mm

Fig. 5 Typical equivalent plastic strain (PEEQ) patterns of models at ultimate load
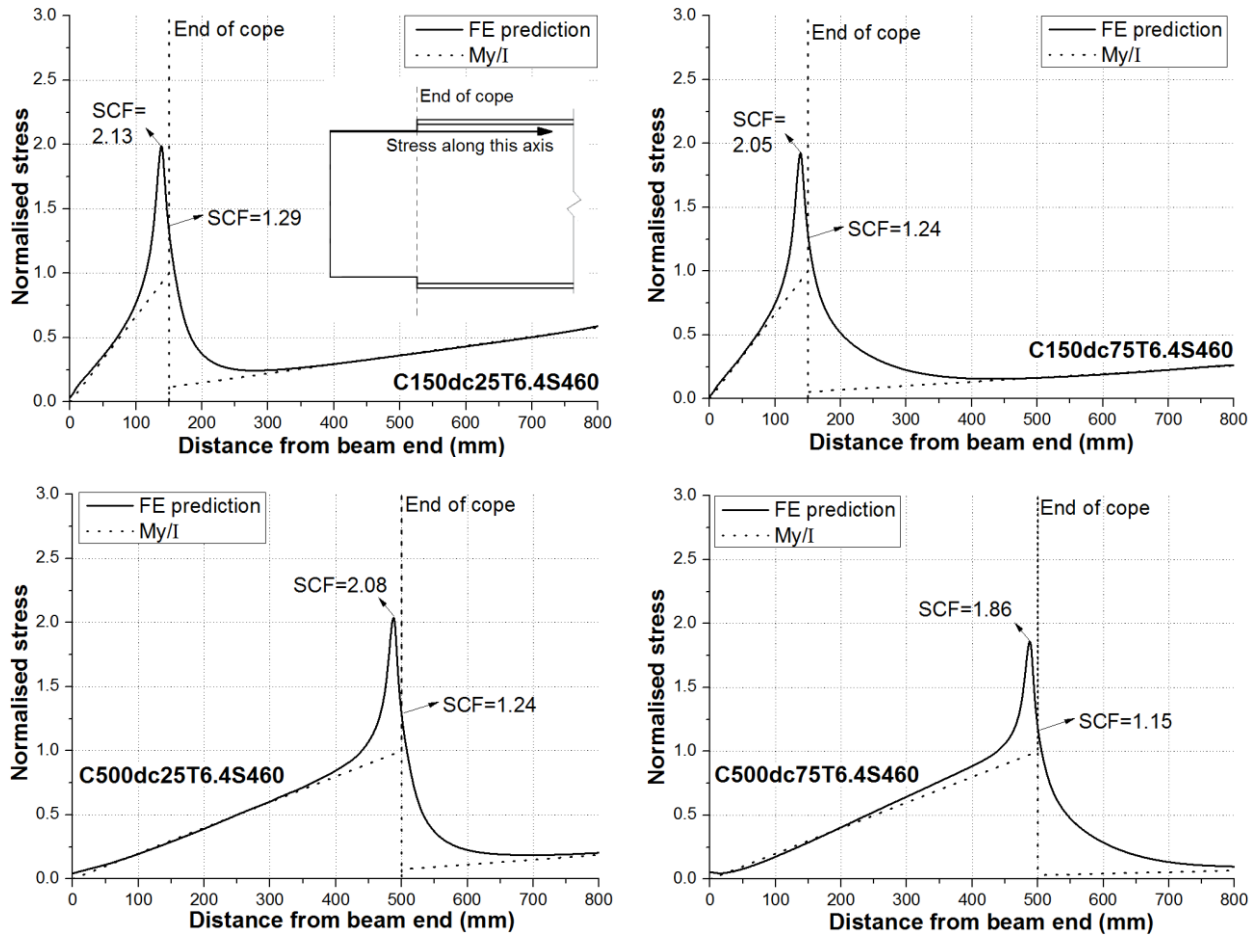
Fig. 6 Typical elastic bending stress distributions along the top cope edge
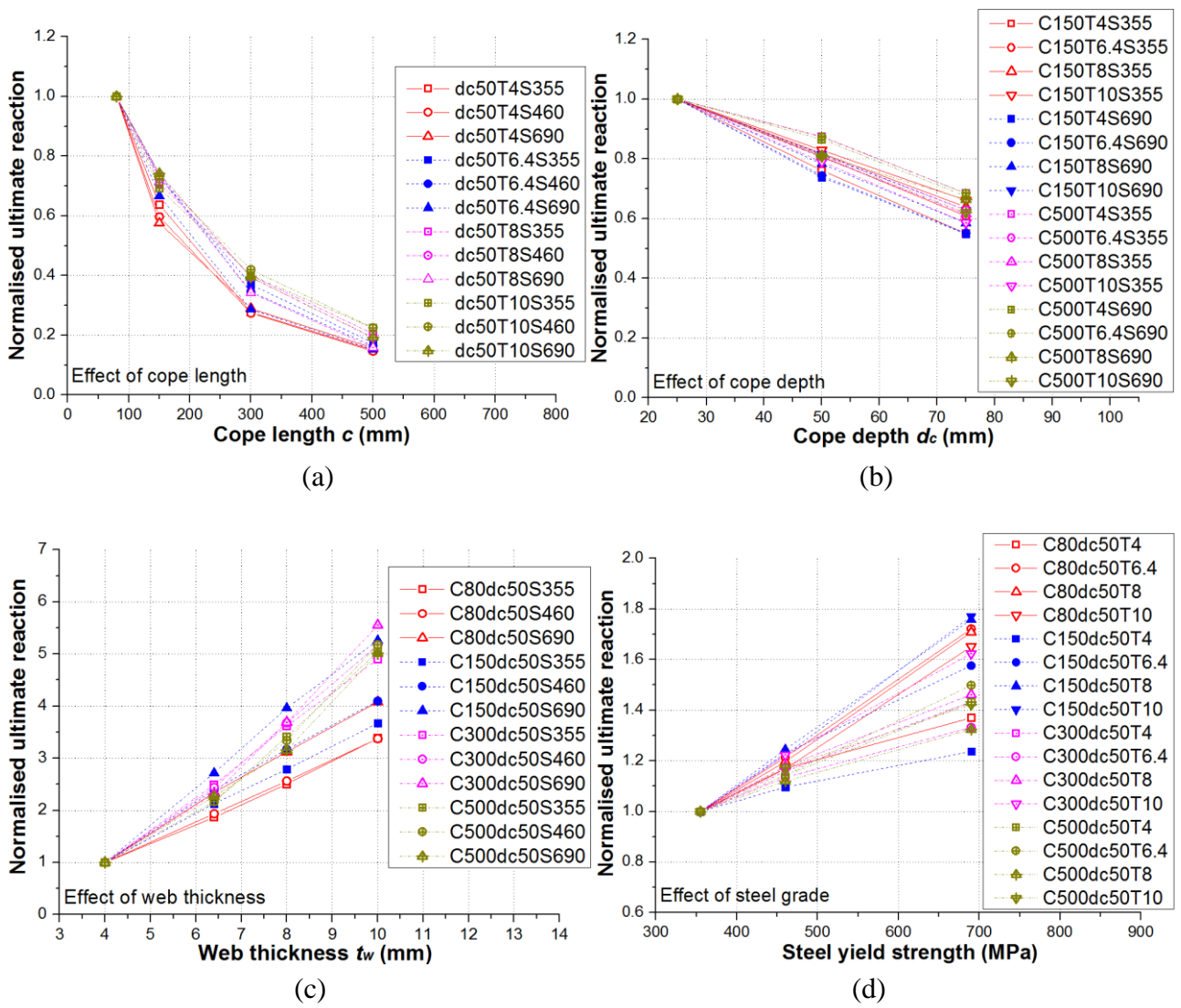
Fig. 7 Influence of parameters on ultimate reaction: a) influence of cope length, b) influence of cope depth, c) influence of web thickness, d) influence of steel grade
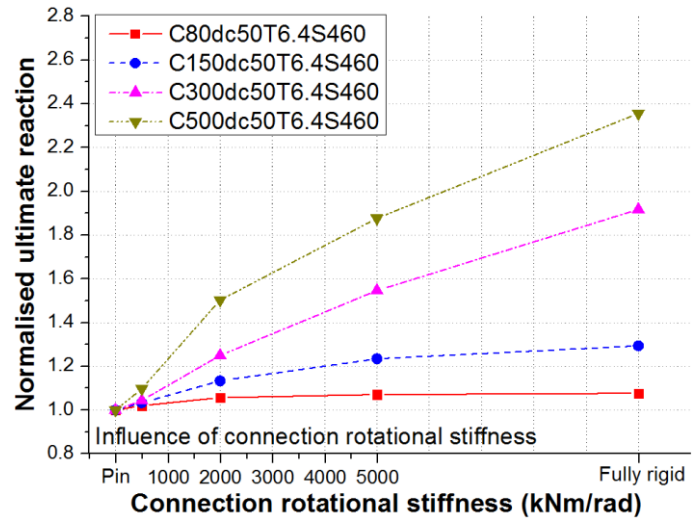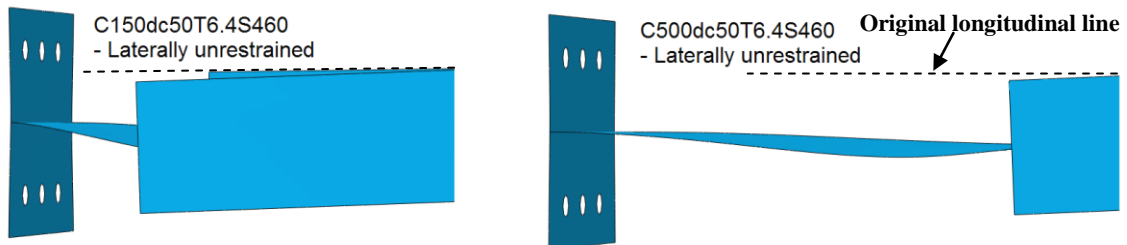
(a)
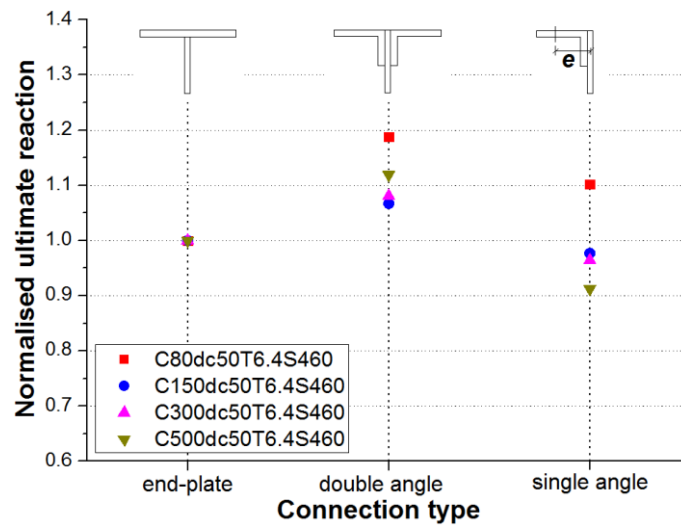
(b)
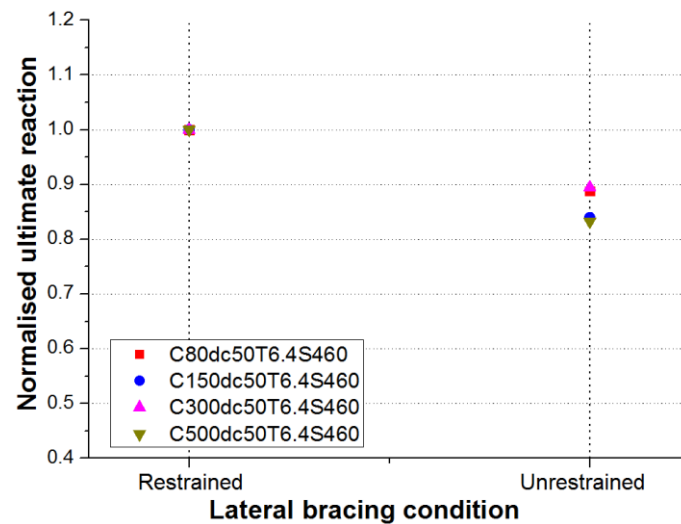
(c)

Fig. 8 Further discussions: a) influence of connection rotational stiffness, b) influence of connection type, c) influence of lateral bracing
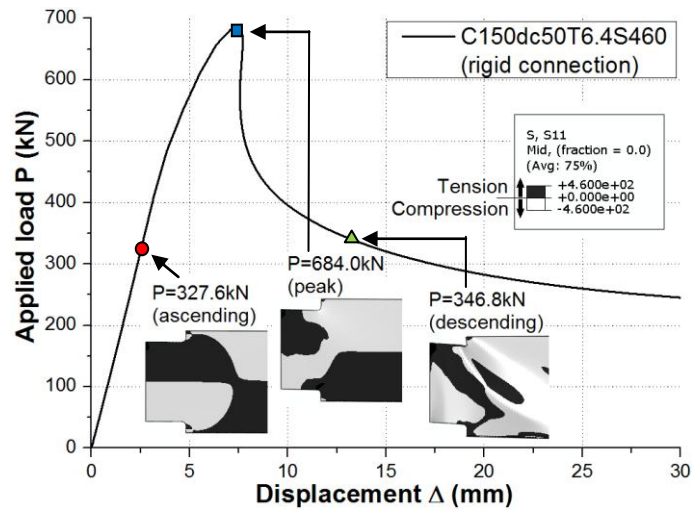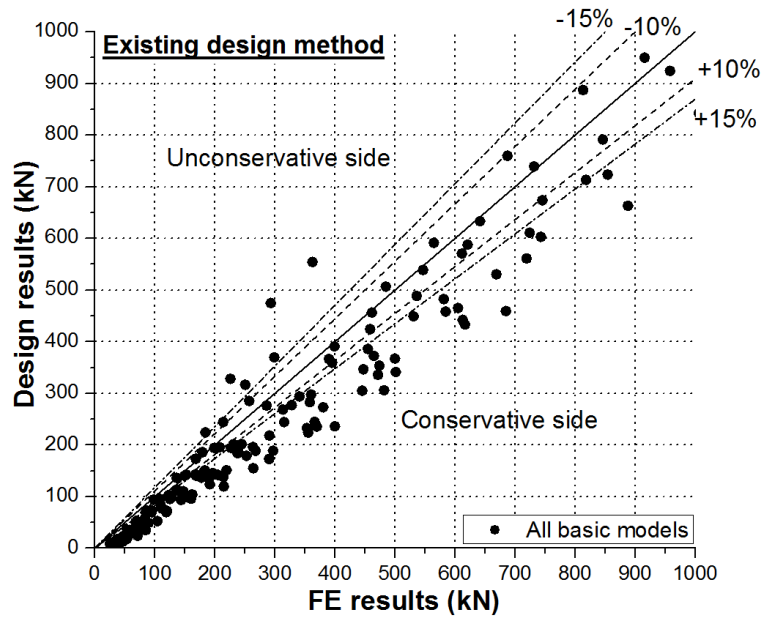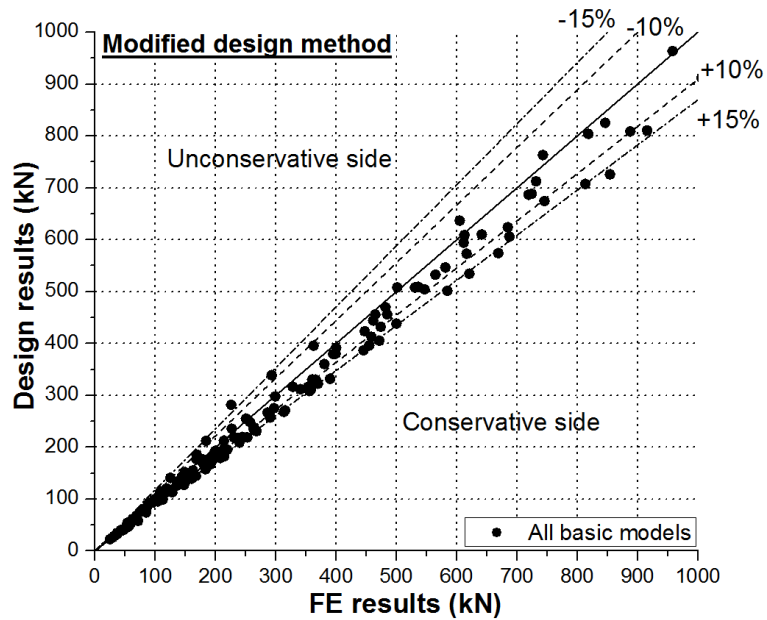
(a)
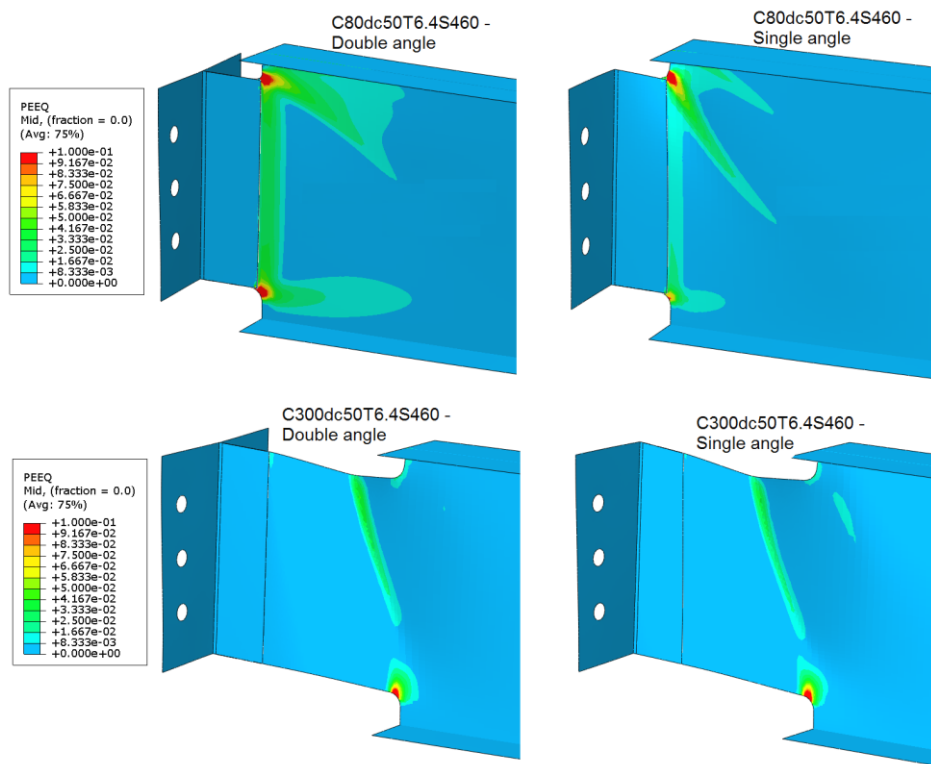
(b)

(c)

Fig. 9 Illustrations for further discussions: a) influence of connection rotational stiffness, b) influence of connection type, c) influence of lateral bracing

(a)

(b)

Fig. 10 Comparisons between FE results and design predictions: a) conventional design method, b) modified design method